NeuroImage 84 (2014) 453–465

Contents lists available at ScienceDirect

NeuroImage

journal homepage: www.elsevier.com/locate/ynimg

The mid-fusiform sulcus: A landmark identifying both cytoarchitectonic and functional divisions of human ventral temporal cortex

Kevin S. Weiner [a,*], Golijeh Golarai [a], Julian Caspers [c,d,g], Miguel R. Chuapoco [a], Hartmut Mohlberg [d], Karl Zilles [d,e,f], Katrin Amunts [c,d], Kalanit Grill-Spector [a,b]

[a] Department of Psychology, Stanford University, Stanford, CA 94305, USA
[b] Neuroscience Institute, Stanford University, Stanford, CA 94305, USA
[c] C. and O. Vogt Institute for Brain Research, Heinrich Heine University Düsseldorf, 40001 Düsseldorf, Germany
[d] Institute for Neuroscience and Medicine (INM-1), Research Centre Jülich, 52425 Jülich, Germany
[e] JARA-BRAIN, Jülich–Aachen Research Alliance, 52425 Jülich, Germany
[f] Department of Psychiatry, Psychotherapy and Psychosomatics, RWTH Aachen University, 52074 Aachen, Germany
[g] Department of Diagnostic and Interventional Radiology, University Düsseldorf, Medical Faculty, D-40225 Düsseldorf, Germany

ARTICLE INFO

Article history:
Accepted 29 August 2013
Available online 8 September 2013

Keywords:
Cytoarchitectonics
Fusiform gyrus
Mid-fusiform sulcus
Eccentricity bias
Fusiform face area

ABSTRACT

Human ventral temporal cortex (VTC) plays a pivotal role in high-level vision. An under-studied macroanatomical feature of VTC is the mid-fusiform sulcus (MFS), a shallow longitudinal sulcus separating the lateral and medial fusiform gyrus (FG). Here, we quantified the morphological features of the MFS in 69 subjects (ages 7–40), and investigated its relationship to both cytoarchitectonic and functional divisions of VTC with four main findings. First, despite being a minor sulcus, we found that the MFS is a stable macroanatomical structure present in all 138 hemispheres with morphological characteristics developed by age 7. Second, the MFS is the locus of a lateral–medial cytoarchitectonic transition within the posterior FG serving as the boundary between cytoarchitectonic regions FG1 and FG2. Third, the MFS predicts a lateral–medial functional transition in eccentricity bias representations in children, adolescents, and adults. Fourth, the anterior tip of the MFS predicts the location of a face-selective region, mFus-faces/FFA-2. These findings are the first to illustrate that a macroanatomical landmark identifies both cytoarchitectonic and functional divisions of high-level sensory cortex in humans and have important implications for understanding functional and structural organization in the human brain.

Introduction

Human ventral temporal cortex (VTC) plays a pivotal role in perceptual and cognitive tasks spanning high-level vision (Haxby et al., 2000; Malach et al., 2002; Martin, 2007; Op de Beeck et al., 2008; Tarr and Gauthier, 2000; Weiner and Grill-Spector, 2013), memory (Henson et al., 2000; Wagner et al., 1999), and multi-sensory integration (Amedi et al., 2002; James et al., 2002; Kitada et al., 2009). One of the most replicable organizational features of human VTC documented by functional magnetic resonance imaging (fMRI) is a large-scale lateral–medial functional distinction. For instance, inanimate (Mahon and Caramazza, 2009; Martin, 2007), place (Aguirre et al., 1998; Epstein and Kanwisher, 1998; Nasr et al., 2011), and peripherally-biased (Hasson et al., 2002; Levy et al., 2001; Malach et al., 2002) representations are located in medial VTC encompassing the medial FG and collateral sulcus (CoS), while animate (Connolly et al., 2012; Mahon and Caramazza, 2009; Martin, 2007), face (Kanwisher et al., 1997), and foveally-biased (Hasson et al., 2002; Levy et al., 2001; Malach et al., 2002) representations are located in lateral VTC, encompassing the lateral fusiform gyrus (FG) and occipito-temporal sulcus (OTS). Intriguingly, in addition to this lateral–medial functional distinction, a lateral–medial cytoarchitectonic distinction has recently been identified (Caspers et al., 2012). Using novel tools detecting transitions in both cell density and layering across gray matter, Caspers et al. (2012) reported two cytoarchitectonic regions in the posterior aspect of VTC: FG1 and FG2. Macroanatomically, FG1 is located on the medial FG extending into the CoS, while FG2 is located on the lateral FG extending into the OTS. Cytoarchitectonically, FG1 displays a columnar arrangement of small pyramidal cells, while FG2 contains large pyramidal cells in layer III and a prominent layer IV, but no columnar arrangement. If and how these functional and cytoarchitectonic parcellations are related to one another is presently unknown.

A major obstacle preventing the full understanding of cytoarchitectonic and functional correspondences in VTC is that macroanatomical structures are yet to be fully characterized. For instance, an often over-looked feature of VTC is that the FG is divided longitudinally by a minor sulcus referred to as the mid-fusiform sulcus, or MFS (Allison et al., 1999; Nasr et al., 2011; Nobre et al., 1998; Puce et al., 1996; Weiner and Grill-Spector, 2010, 2012, 2013; Weiner et al.,

* Corresponding author.
E-mail address: kweiner@stanford.edu (K.S. Weiner).

1053-8119/$ – see front matter © 2013 Elsevier Inc. All rights reserved.
http://dx.doi.org/10.1016/j.neuroimage.2013.08.068

2010). Indeed, although the MFS was first labeled as such in the late nineties (Allison et al., 1999; Nobre et al., 1998; Puce et al., 1996), it has been mentioned in the literature less than ten times (Davidenko et al., 2012; Nasr et al., 2011; Parvizi et al., 2012; Schultz et al., 2003; Weiner and Grill-Spector, 2010, 2012, 2013; Weiner et al., 2010). Despite the paucity of studies mentioning the MFS, recent research in adults provides insight into how incorporating the MFS into functional neuroimaging might enhance the understanding of VTC functional organization. Specifically, these studies show that the MFS serves as a lateral–medial functional boundary dividing face-selective regions (Davidenko et al., 2012; Nasr et al., 2011; Parvizi et al., 2012; Weiner and Grill-Spector, 2010, 2012, 2013; Weiner et al., 2010) from place-selective regions (Nasr et al., 2011), and also dissociates differential repetition suppression mechanisms (Weiner et al., 2010). However, it is unknown (1) if the morphology of the MFS is stable across development, (2) if the MFS is coupled with cytoarchitectonic partitions of VTC, (3) whether the MFS predicts additional lateral–medial functional gradients in VTC such as eccentricity bias representations, and (4) if the MFS also predicts the fine-scale clustering of face-selective regions.

To address these questions, we conducted four separate studies. First, we characterized the morphology of the MFS in 69 subjects (ages 7–40), determining the developmental and stable features of the MFS in children, adolescents, and adults. Second, we examined the relationship between the MFS and cytoarchitectonic regions FG1 and FG2 using an independent set of 10 postmortem brains. Third, using a novel classification approach, we tested if the MFS serves as a functional boundary separating the large-scale eccentricity bias map (Hasson et al., 2002; Levy et al., 2001; Malach et al., 2002) in 36 subjects (ages 7–40). We chose eccentricity bias measurements because they show a medial–lateral gradient across VTC and constitute a large-scale category-independent representation. Fourth, we tested if the MFS serves as a functional landmark identifying the fine-scale functional organization of face-selective regions pFus-faces/FFA-1 and mFus-faces/FFA-2 (Weiner and Grill-Spector, 2010) using high-resolution fMRI (HR-fMRI) in 14 adult subjects. To our knowledge, this is the first in depth analysis of human high-level visual cortex spanning cytoarchitectonics, macroanatomy, and functional organization at multiple spatial scales. We demonstrate that the MFS is a stable macroanatomical feature across development, as well as a crucial landmark identifying both cytoarchitectonic and functional divisions of VTC.

Materials and methods

We describe the methods in two sections, one for the anatomical and functional MRI scans and a separate section for the cytoarchitectonical analysis.

Participants

To obtain macroanatomical data, 69 subjects participated in an anatomical MRI session. Subjects included 20 children (ages 7–11, 7 females), 14 adolescents (ages 12–17, 8 females), and 35 adults (ages 18–40, 18 females), all of whom were healthy with no report of neurological or psychiatric disease. To obtain data on the functional organization of VTC, 36 (12 children, 12 adolescents, and 12 adults) of these 69 subjects also participated in an fMRI session. Written consent was obtained from each subject. Procedures were approved by the Stanford Internal Review Board on human subjects research.

Anatomical scans and analysis

Scanning. All subjects were scanned on a GE 3-Tesla Signa scanner at Stanford University. A high-resolution anatomical volume of the whole brain was acquired with a whole head coil using a T1-weighted SPGR pulse sequence (TR = 1000 ms, flip angle = 45°, 2 NEX, FOV = 200 mm, resolution of 0.78 × 0.78 × 1.2 mm).

Data analysis. Data were analyzed with MATLAB (MathWorks) using the mrVista toolbox (http://white.stanford.edu/software).

Cortical surface reconstruction. Anatomical volumes were aligned to the AC-PC plane and resampled to 1 mm isotropic voxels. Using a combination of automated (FreeSurfer: http://surfer.nmr.mgh.harvard.edu) and manual segmentation tools (ITK-SNAP: http://white.stanford.edu/itkgray), each anatomical volume was segmented to separate gray from white matter, from which we reconstructed the cortical surface for each subject (Wandell et al., 2000).

Identification of the MFS on single slices and cortical surface reconstructions. The MFS is a longitudinal sulcus dividing the FG into lateral and medial partitions as viewed on the cortical surface (Fig. 1). Here, we determined the identifying features of the MFS relative to surrounding sulci on single sections in order to define the MFS consistently on anatomical MRIs as well as in single histological sections. As illustrated in Fig. 1, the MFS is positioned between the OTS and CoS on the cortical surface (Fig. 1a), resulting in a distinct omega (ω) pattern on single coronal slices (Fig. 1b). This ω pattern (red outline in Figs. 1–2) is a characterizing feature of the MFS despite differences in how it may appear on the cortical surface.

Sulcal length measurements. Lines were manually drawn along the fundus of the MFS on the cortical surface for each subject and hemisphere. The length of this line was determined using a modified version of Dijkstra's algorithm (as in Wandell et al., 2000). As the cortical surface reconstruction is composed of a series of connected vertices, the algorithm computes the length by determining the shortest path between endpoints on the line taking into consideration their actual distance in gray matter. When the MFS was fractionated into more than one component (Table 1, Fig. 2, and Results), the total length was based on the sum of the independent sulcal components excluding the interspersed

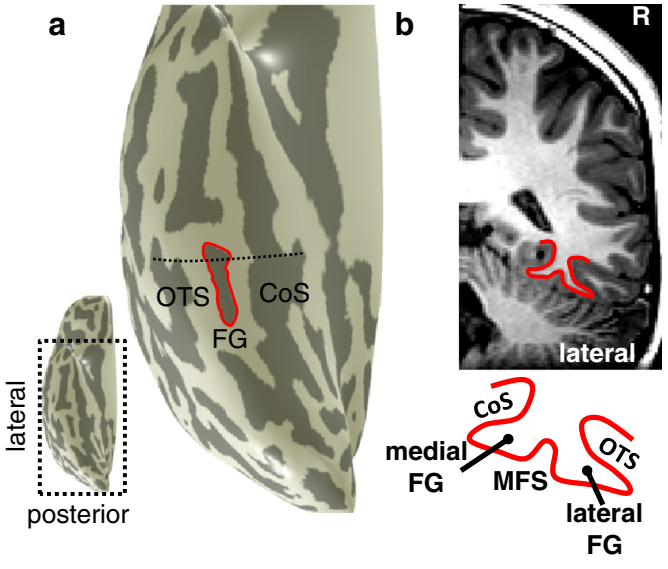

Fig. 1. The mid-fusiform sulcus (MFS). Example right hemisphere from a ten-year old male. (a) Inflated cortical surface with sulci illustrated in dark gray. The MFS (outlined in red) is a longitudinal sulcus dividing the fusiform gyrus (FG) into lateral and medial partitions, flanked by the occipito-temporal sulcus (OTS) laterally and the collateral sulcus (CoS) medially (inset for location of zoomed portion). (b) The MFS, OTS, and CoS have a distinctive ω pattern on single coronal slices where the MFS is the shallower sulcus flanked by the much deeper CoS and OTS. Top: Example coronal slice from the position of the dotted line in (a). Bottom: Schematic of the ω pattern of the MFS, OTS, and CoS.

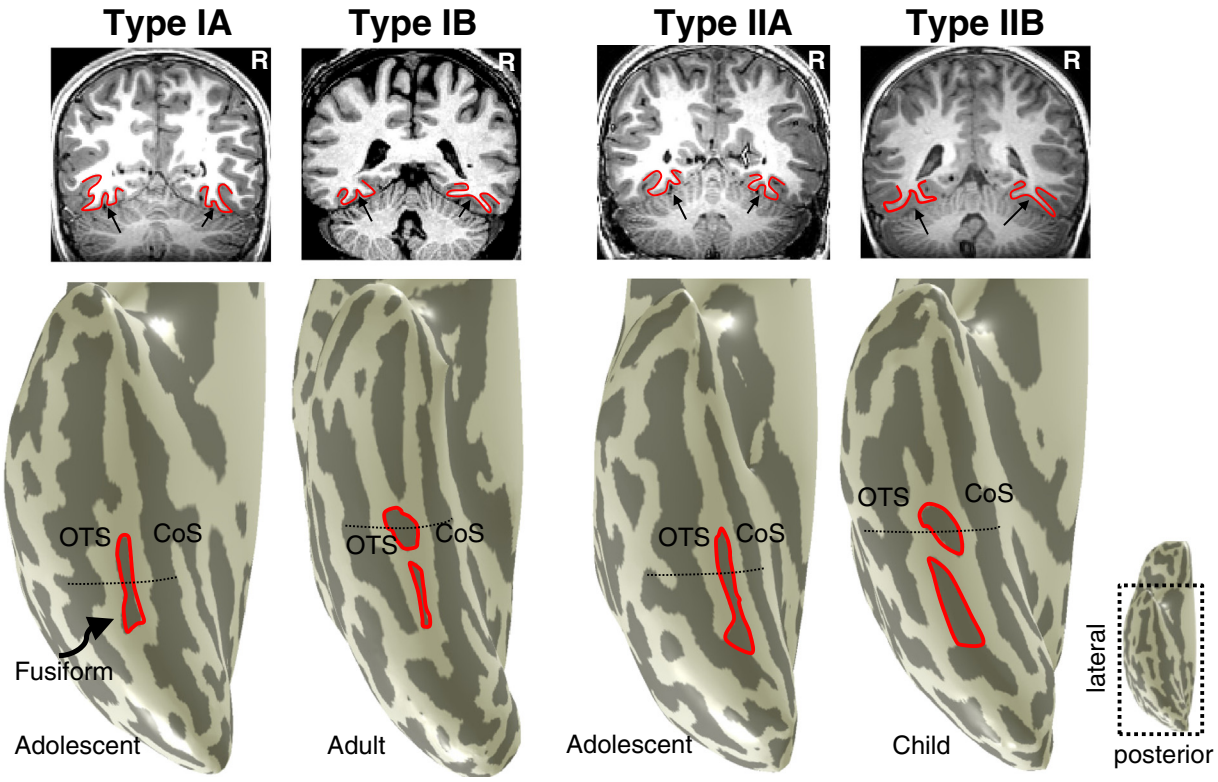

Fig. 2. The four morphological patterns of the MFS. The MFS is outlined in red in both single coronal slices (top) and corresponding inflated hemispheres (bottom). Dotted lines indicate the location of the coronal slice. Note that the ω pattern described in Fig. 1 persists on single coronal slices despite differences in fractionation and/or contiguity with surrounding sulci on the cortical surface. All patterns are equally likely across ages and hemispheres (Table 1). CoS: collateral sulcus; OTS: occipito-temporal sulcus.

gyral components. We repeated the length measurement including the intergyral components, which were on average 5.26 ± 0.22 mm long, but it minimally affected MFS length measurements as these occur in less than 30% of hemispheres (length with intergyral: 29.2 ± 13.5 mm, without intergyral: 27.3 ± 10.8 mm). To further relate these measurements to stereotaxic space, we calculated the Talairach coordinates of the anterior and posterior extents of the MFS in the 70 adult hemispheres (Table 2).

Sulcal depth measurements. Lines were manually drawn from the lateral lip to the medial lip of each sulcus of interest (MFS, OTS, and CoS) on the cortical surface (dotted lines on the cortical surface and corresponding coronal slices in Figs. 1–2). The distance of this line was first determined using the same algorithm as the length measurements and then divided by two to transform these width measurements into depth measurements. To test the validity of this approach, we also measured sulcal depth in coronal slices — evaluating the distance between the fundus of a sulcus (the MFS, CoS, or OTS) to the morphologically closed border of the cerebrum in the 35 adult subjects. In a two-way repeated measures ANOVA with factors method (cortical surface and coronal slices) and sulcus (MFS, CoS, and OTS), there was no significant main effect of method, no main effect of subject, and no significant interaction ($ps > .54$). Thus, we report depth measurements from the cortical surface.

Table 1
Incidence characteristics of the mid-fusiform sulcus (MFS) in the right (RH) and left (LH) hemispheres.

	Child RH	Child LH	Teen RH	Teen LH	Adult RH	Adult LH	Total	Total %
Type IA	9/20	10/20	8/14	2/14	20/35	18/35	67/138	48.55%
Type IB	5/20	5/20	3/14	2/14	5/35	7/35	27/138	19.57%
Type IIA	5/20	3/20	2/14	6/14	7/35	6/35	29/138	21.01%
Type IIB	1/20	2/20	1/14	4/14	3/35	4/35	15/138	10.87%

fMRI scans and analysis

Large-scale functional–structural correspondence. To test if the MFS reliably delineates lateral–medial functional divisions of VTC across development, we examined 12 children (ages 8–11), 12 adolescents (ages 12–16), and 12 adults (ages 18–40) using fMRI. During fMRI, subjects viewed images of faces and houses presented either centrally spanning 3° or peripherally in a ring whose inner radius was 7° and outer radius was 14°. Stimuli in the periphery were scaled in size to account for lower acuity in the peripheral visual field and their diameter was ~6°. Subjects participated in 2 runs of this experiment where each run was 384 s long containing four, 12-second blocks of each condition. Subjects were instructed to fixate on a central dot and to indicate with a button press when the fixation color changed.

Acquisition. We acquired 32 slices at a resolution of 3.125 × 3.125 × 3 mm mm using a two-shot T2*-sensitive spiral acquisition

Table 2
Talairach coordinates of the anterior and posterior tips of the MFS in the adult brain (n = 35).

	x	*y*	*z*
Anterior			
Right (ave ± std)	32 (3.79)	−41 (6.40)	−16 (4.19)
Left (ave ± std)	−31 (3.50)	−40 (6.18)	−17 (3.76)
Posterior			
Right (ave ± std)	28 (4.61)	−59 (8.38)	−13 (5.46)
Left (ave ± std)	−30 (3.94)	−62 (7.88)	−15 (3.74)

sequence (Glover, 1999) (FOV = 200 mm; TR = 2 s, TE = 30 ms, and flip angle = 77°) on a 3 T GE scanner. Inplane anatomical scans were acquired with the same prescription using a two-dimensional RF-spoiled GRASS (SPGR) sequence (TE = 1.9 ms, flip angle = 15°, bandwidth = 15.63 kHz).

Time series processing. Functional data of each session were motion corrected using an affine transformation (Nestares and Heeger, 2000). Time series data were filtered using a temporal high-pass filter with a 1/20 Hz cutoff and then converted to percentage signal change by dividing the time series of each voxel by its mean intensity. We estimated the blood oxygen level dependent (BOLD) response amplitudes for each condition using a general linear model (GLM) applied to the time series of each voxel using as predictors the experimental conditions convolved with the hemodynamic impulse response function used in SPM5. Data were not spatially smoothed.

Anatomical ROIs. Lateral and medial anatomical VTC regions of interest (ROIs) were defined on the cortical surface of each subject and hemisphere, blind to functional data. The anterior and posterior boundaries of each ROI were the anterior and posterior extents of the MFS, respectively. Lateral VTC was defined as the region between the lateral lip of the MFS and OTS. Medial VTC was defined as the region between the medial lip of the MFS and CoS (Fig. 7a). The average sizes of lateral and medial anatomical ROIs were similar across age groups (children: 2600 $mm^3 \pm 158$ mm^3; adolescents: 2580 $mm^3 \pm 151$ mm^3; adults: 2380 $mm^3 \pm 126$ mm^3; no significant effect of age, $p = .47$).

Linear discriminant analysis (LDA) of functional–structural correspondence. To test if the MFS serves as a functional landmark in VTC, we conducted a linear discriminant analysis (LDA) to examine if the *anatomical* location of each voxel (i.e. whether it belonged to the lateral or medial VTC) in one subject's brain could be classified from the *functional* data in other subjects' brains. For each ROI and hemisphere, we used 500 voxels whose time series were best fit by the GLM. This voxel selection criterion was implemented to be independent of stimulus condition and to exclude voxels with excessive noise. Within-group classification was conducted with a leave-one-subject-out procedure. Across-group classification was conducted by training on one age group and testing on subjects from another age group. The training set consisted of eccentricity bias values measured at the level of each voxel (*t*-value of fovea–periphery, collapsed across stimulus categories) labeled as belonging to either the lateral or medial VTC ROIs. We used an LDA to derive a linear boundary separating these *t*-values based on their anatomical classification. The test set consisted of functional *t*-values from voxels with an unknown anatomical location from a subject not used in the training. Using the boundary derived from the training set, we classified the test set voxels to either the lateral or medial VTC ROI. Classification performances on test sets were evaluated by comparing the classification results to the actual anatomical location of each voxel, and then calculating the percentage of voxels classified correctly. Since there was no effect of hemisphere on classification performance ($p = .23$), data were concatenated across hemispheres resulting in 1000 voxels from each subject used for classification.

Distance between eccentricity bias boundary and the MFS fundus. Following the classification analyses, which were blind to the functional data, we measured the distance along the cortical surface between each point of the eccentricity bias boundary in VTC (defined as the transition between foveally-biased and peripherally-biased voxels) and the MFS fundus, and calculated the average distance in each hemisphere. Unlike the classification analysis, this analysis included voxels within the MFS itself to measure the exact position of the functional transition within the MFS. In Fig. 8, we show the average distance between the eccentricity bias boundary and the MFS fundus collapsed across hemispheres and subjects for each age group.

Fine-scale functional–structural correspondence. To examine the MFS-functional coupling in the anterior–posterior dimension, 14 of the 35 adults were scanned with high-resolution fMRI (HR-fMRI) during a block design experiment while viewing images of different categories including faces, limbs, objects, houses and texture patterns as described in prior studies (Parvizi et al., 2012; Weiner and Grill-Spector, 2010, 2011; Weiner et al., 2010). HR-fMRI improves localization of functional regions and improves measurements of the anterior portion of the MFS, where the timeseries signal-to-noise ratio is often low due to the ear canal susceptibility artifact (Weiner and Grill-Spector, 2013).

Acquisition. Data were collected on a 3 T GE scanner with either a 32-channel surface coil, EPI sequence, and 1.8 mm isotropic voxels (FOV = 192 mm; TR = 2 s, TE = 30 ms, and flip angle = 77°, 28 slices; 7 subjects) or 8-channel surface coil, spiral acquisition sequence, and 1.5 × 1.5 × 3 mm voxels (FOV = 192 mm; TR = 2 s, TE = 30 ms, and flip angle = 77°, 12 slices, 7 subjects). As there was no effect of acquisition on the MFS-functional coupling reported in Figs. 9–10 (1-way ANOVA with factor of acquisition; p = .71), we report results averaged across all 14 subjects.

Analysis. To determine the structural–functional coupling between the MFS and face selectivity using HR-fMRI, we defined anatomical, Talairach, and functional ROIs for each subject and hemisphere. *Anatomical ROIs*: 1 cm disk ROIs were placed on the anterior and posterior extents of the MFS extending laterally into the FG (Fig. 10). *Talairach ROIs*: 1 cm disk ROIs were centered on the Talairach coordinates of FFA-1 and FFA-2 from prior studies (Pinsk et al., 2009). *Functional ROIs*: pFus-faces/FFA-1 and mFus-faces/FFA-2 were defined as voxels in the FG responding more to faces > nonfaces, $t > 3$, voxel level, uncorrected (see Davidenko et al., 2012; Parvizi et al., 2012; Weiner and Grill-Spector, 2010, 2011, 2013; Weiner et al., 2010). We examined the percentage overlap between these anatomical and functional ROIs as well as Talairach and functional ROIs in each subject.

Postmortem data acquisition and analysis

To examine the relationship between the MFS and cytoarchitectonic divisions of the FG, 10 postmortem (PM) brains were studied. These brains were from adults (ages 37–85, 5 females) with no history of neurological or psychiatric disease (with the exception of one individual with transitory motor disease. See Table 1 from Amunts et al., 2000; Caspers et al., 2012; Rottschy et al., 2007). All 10 PM brains came from the body donor program of the Institute of Anatomy, University of Dusseldorf, all procedures were approved and in alignment with the program guidelines (Amunts et al., 2000).

Scanning

Postmortem brains were scanned on a Siemens 1.5 T Scanner (Erlangen, Germany) after being removed from the subject's skull 8–24 h after death.

Anatomical brain volumes

A high-resolution anatomical volume of the whole brain was acquired using a T1-weighted 3D-FLASH sequence (TR = 40 ms, flip angle = 40°, TE = 5 ms; resolution of 1 × 1 × 1 mm) before histological processing and after fixation in 4% formalin or Bodian's fixative for at least 6 months.

Cortical surface reconstruction

Detailed methods of histology and 3D reconstruction have been described previously (Amunts et al., 1999, 2005; Zilles et al., 2002). The fixated brains were embedded in paraffin, serially sectioned in coronal sections (20 μm thick), and stained with the Merker-method for cell bodies (Merker, 1983). This method yields a high contrast between cell bodies (black) and the neuropil (unstained). 3D reconstructions were computed using (a) the 3D-MRI volume of each brain, (b) images of the paraffin block face for precise alignment of the histological sections, and (c) digitized images of the cell body-stained sections (Amunts et al., 2004). For direct comparison to the 69 subjects, brains

were also manually segmented to separate gray from white matter using ITK-SNAP (http://white.stanford.edu/itkgray), from which we reconstructed the cortical surfaces (Fig. 6a).

Detection of FG1 and FG2 boundary

A detailed description for defining cytoarchitectonic areas of FG1 and FG2 is given elsewhere (Amunts and Zilles, 2001; Amunts et al., 2000; Caspers et al., 2012). Briefly, the border between FG1 and FG2 was defined (Caspers et al., 2012) using a statistically testable, quantitative, and observer-independent cortical parcellation technique (Amunts et al., 2000; Schleicher et al., 1999, 2005; Zilles et al., 2002). Specifically, gray-level indices (GLI) were determined in digitized histological sections as a measure of the volume proportion between cell bodies and the neuropil. GLI profiles were calculated along curvilinear trajectories oriented perpendicular to the cortical layers, thus measuring the GLI from the superficial to the innermost layer in cortical regions of interest. The shape of GLI profiles was determined based on ten features: the mean GLI value, the position of the center of gravity on the profile curve (cortical depth), the standard deviation of the mean GLI (indicating the variability of the GLI throughout all layers), skewness and kurtosis of the profile curve, and the respective features from the profile's first derivative (Schleicher et al., 1999). The borders between areas were determined based on the cortical position of the greatest difference between neighboring GLI profiles quantified by the Mahalanobis distance and tested for significance (Fig. 4; Hotelling's T^2 test; Bonferroni-corrected). Areal borders are expected at positions along the cortical ribbon showing a great dissimilarity in laminar patterns between adjacent blocks of profiles. To assure that the areal boundary was not dependent on the block size, the procedure was titrated for block sizes ranging from 8 to 24 profiles per block. Cortical borders were confirmed if they were consistently positioned in adjacent histological sections and across several block sizes (Fig. 4).

Distance between the FG1/FG2 boundary and the MFS

In all 20 hemispheres, we measured the distance along the cortical surface between each point of the FG1/FG2 boundary and the nearest point on the MFS in a given hemisphere. We used the average distance for each subject in each hemisphere as our measure of the distance between the FG1/FG2 boundary and the MFS and report the mean distance across subjects. In the 18 hemispheres within which the cytoarchitectonic boundary between FG1 and FG2 occurred in the MFS, we also measured the percentage of the MFS containing the FG1/FG2 boundary (Fig. 6b) and the average distance of this boundary from the fundus of the MFS (Fig. 6c).

Relationship between Talairach coordinates and the FG1/FG2 boundary

Using the average Talairach coordinates of the MFS from our independent adult sample (Table 2), we compared the ability of Talairach coordinates to predict the FG1/FG2 boundary relative to the actual MFS coordinates. In all 20 hemispheres, we drew a line between the anterior and posterior points of the MFS as predicted by Talairach coordinates. We then measured the average distance between this line and the FG1/FG2 boundary and compared this metric to the distance between the FG1/FG2 boundary and the MFS as described in the above section.

Results

Incidence, morphology, and development of the mid-fusiform sulcus (MFS)

The MFS displays four morphological patterns and is identifiable in every hemisphere

We first examined the incidence and morphological features of the MFS on the cortical surface and single coronal slices in 138 hemispheres across three age groups: children, adolescents, and adults. Although the MFS is a minor sulcus and not mentioned in the most commonly used human neuroanatomical atlases from the last century (Brodmann, 1909; Duvernoy, 1999; Evans et al., 1992; Ono et al., 1990; Talairach and Tournoux, 1988), it was identifiable in all 138 hemispheres, and is best described as a longitudinal sulcus dividing the FG into lateral and medial partitions (Fig. 1) with a distinctive "ω" pattern on single coronal slices (red outline in Figs. 1–2).

The organization of the MFS relative to surrounding sulci exhibited two characteristic pattern types (Type I and Type II) that were evident when viewing the cortical surface. In Type I patterns, the MFS appeared as a distinct sulcus separate from the OTS and CoS. In Type II patterns, the MFS intersected with either the OTS or CoS. Both Type I and Type II patterns were further classified based on whether the MFS was continuous (subtype A) or fractionated (subtype B). Thus, the features of the different MFS patterns are defined as follows:

Type IA: a single longitudinal sulcus, distinct from the OTS and CoS (Fig. 2, far left).
Type IB: a fractionated longitudinal sulcus, distinct from the OTS and CoS (Fig. 2, middle left).
Type IIA: a single longitudinal sulcus, sharing a sulcal bed with the OTS or CoS (Fig. 2, middle right).
Type IIB: a fractionated longitudinal sulcus, with at least one component sharing a sulcal bed with the OTS or CoS (Fig. 2, far right).

These morphological patterns occurred with similar frequencies across hemispheres, genders, and age groups tested (Table 1). Type I MFS patterns (manifesting as a distinct sulcus) were the most common, occurring in about two-thirds (68%) of hemispheres. Type II MFS patterns occurred in about a third of hemispheres (32%) and were distinct from the recently described lateral branches of the CoS (Huntgeburth and Petrides, 2012). Further, unfractionated A patterns were about two times as frequent as fractionated B patterns (ratio: 2.5 for Type I; 1.9 for Type II) and fractionated B patterns were most frequently composed of two components (34/42; 81%). Thus, the MFS is a stable anatomical landmark on the FG with four typical morphological patterns that are common across hemispheres, genders, and age groups.

Characteristic feature of the MFS: half as deep as the OTS and CoS

The average depth of the MFS was 6.13 ± 1.53 mm in children, 6.0 ± 0.91 mm in adolescents, and 6.57 ± 1.67 mm in adults (Fig. 3). There was no difference in depth (a) across hemispheres within any of the age groups (all $ps > .67$; paired t-tests), (b) across groups (1-way ANOVA; $F(2,68) = .94$, $p = .39$), or (c) across genders (1-way ANOVA, $F(1,68) = .31$, $p = .58$). There was also no correlation between age and MFS depth in either hemisphere (all $rs < .16$, all $ps > .2$).

The MFS exhibited two features distinguishing it from the OTS and CoS. First, the MFS was significantly more shallow than both sulci (1-way repeated measures ANOVA: $F(2,206) = 562$, $p < 10^{-10}$; Fig. 3). In fact, the OTS and CoS were more than two times as deep as the MFS (average ratio OTS/MFS = 2.13, and CoS/MFS = 2.16). Second, depth measurements of the MFS in one hemisphere were correlated with depth measurements in the other ($r = .28$, $p < .02$, collapsed across groups), which was not the case for the OTS or CoS (all $rs < .11$, all $ps > .35$). Taken together, the shallowness of the MFS relative to the OTS and CoS is a stable measurement across subjects and is predictable across hemispheres within a given subject.

Length of the MFS is consistent across age groups and hemispheres

The length of the MFS was on average 25.7 ± 8.0 mm in children, 28.8 ± 6.0 mm in adolescents, and 27.5 ± 10.3 mm in adults. There were no differences in MFS length (a) across hemispheres within age group (all $ps > .28$; paired t-tests), (b) across groups (1-way ANOVA: $F(2,68) = .51$; $p = .60$), or (c) across genders (1-way ANOVA, $F(1,68) = .02$, $p = .89$). Furthermore, there was no correlation between age and MFS length in either hemisphere (all $rs < .16$, all $ps > .2$), or between MFS length in the right and left hemisphere ($r = .02$, $p = .88$).

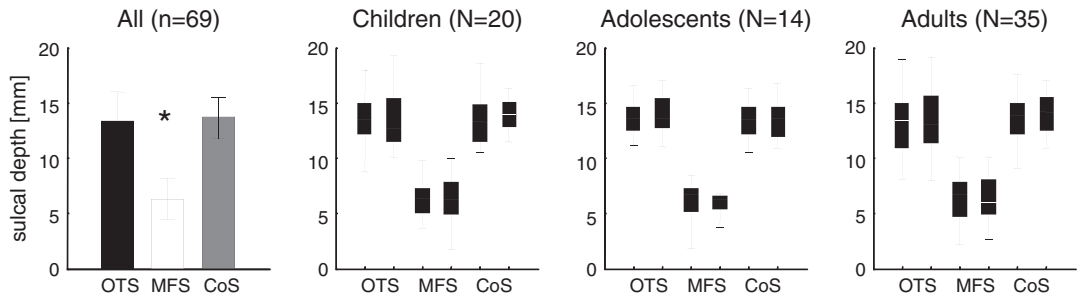

Fig. 3. The CoS and OTS are more than two times as deep as the MFS. Leftmost panel: Each bar (± std) represents data averaged across hemispheres and subjects. The MFS is significantly more shallow than either the OTS or CoS, *$p < 10^{-38}$. Right panels: Boxplots of MFS depth indicating median, 25% and 75% percentiles, as well as range of minimum and maximum values separately for each age group. In each pair, the right hemisphere measurements are presented on the right.

In contrast to the MFS depth, there was significant variability across subjects in the length of the MFS, ranging from 2.0 mm to 56.3 mm. This variability is consistent with prior reports (8 mm to 54 mm in 17 subjects; Nasr et al., 2011). Morphologically, this variability in length affected the posterior, but not anterior, limit of the MFS, where the anterior tip of the MFS was a stable macroanatomical landmark situated about halfway between the tips of the temporal and occipital poles (Fig. 2). However, the posterior extent of the MFS varied substantially across subjects. Indeed, the largest variability among Talairach coordinates of the MFS occurs in the y-dimension of the posterior MFS (Table 2).

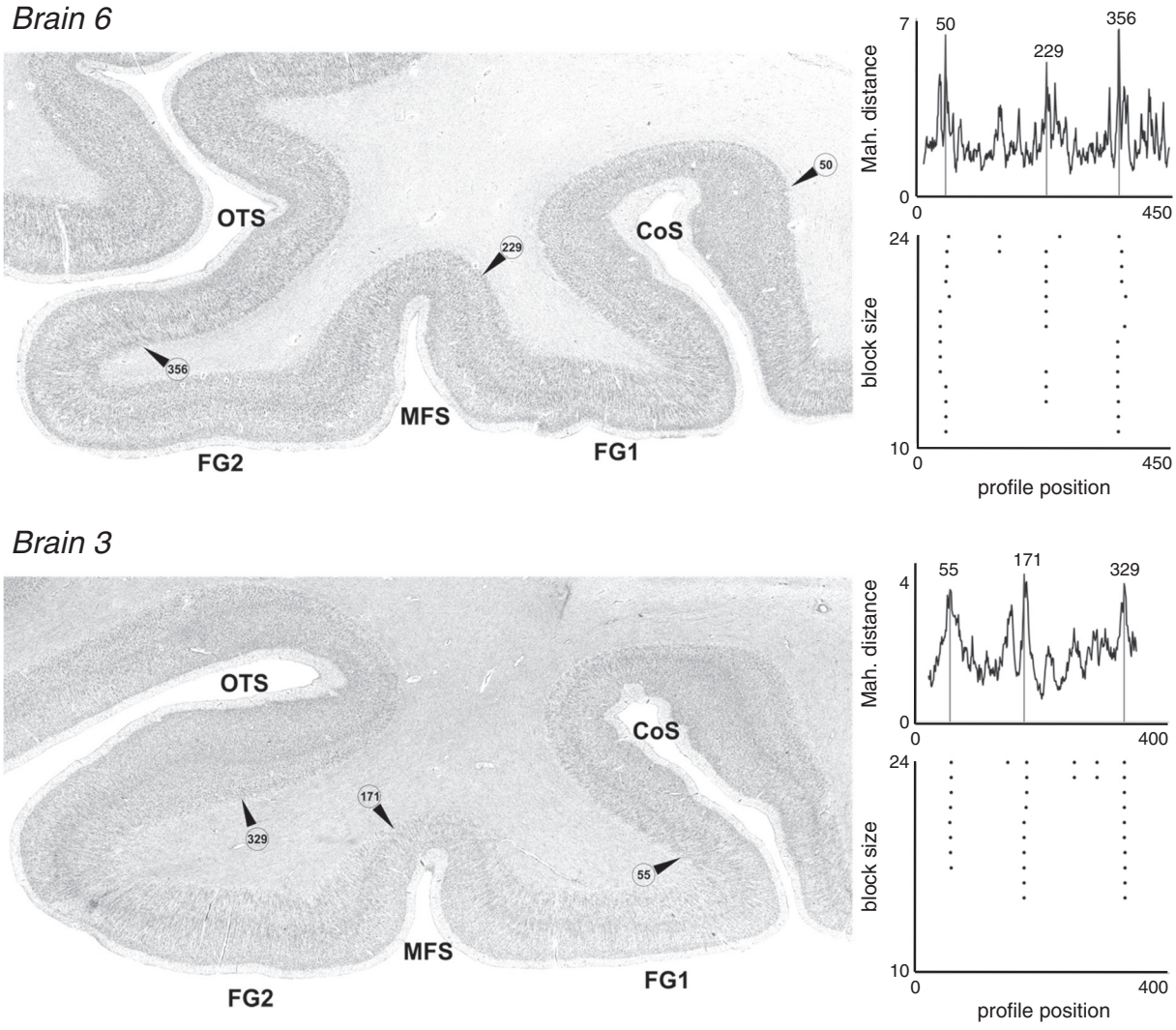

Fig. 4. Cell body stained histological coronal sections through the fusiform gyrus of two different adult brains show that the boundary between FG1 and FG2 is in the MFS. Arrowheads with numbers indicate the positions of the cytoarchitectonically defined borders between FG1 and FG2 as well as between these areas and the surrounding cortex. The course of the Mahalanobis distance along the cortical ribbon is shown by the black curves on the right side of the figure. The respective graphs below the Mahalanobis curves demonstrate the independence of the position of the three significant Mahalanobis distances from the block size comprising immediately neighboring laminar profiles (for details of the observer-independent detection of areal boundaries see Materials and methods: Detection of FG1 and FG2 boundary). Acronyms: CoS: collateral sulcus; FG1 and FG2 are cytoarchitectonical areas; MFS: mid-fusiform sulcus; OTS: occipito-temporal sulcus.

Cytoarchitectonics

The boundary between cytoarchitectonic regions FG1 and FG2 occurs within the MFS

We next examined the location of the MFS relative to two cytoarchitectonic divisions of the FG, FG1 and FG2, in 10 postmortem (PM) brains whose cytoarchitectonics were defined previously (Caspers et al., 2012). The border between FG1 and FG2 was determined based on the cortical position of the greatest difference between neighboring GLI profiles quantified by the Mahalanobis distance and tested for significance (Materials and methods; Fig. 4). It is important to note that these cytoarchitectonic boundaries were defined using observer independent methods, and were made prior to characterizing the MFS, as the ω pattern (Fig. 1) used to localize the MFS on single histological sections was unknown at the time of the original FG1/FG2 identification (Caspers et al., 2012).

We identified the presence of the MFS on digitized images of histological sections (20 μm thick), using the typical ω pattern of the MFS relative to the OTS and CoS. The difference in depth between the MFS relative to the CoS and OTS producing the ω pattern is a robust metric, where the CoS and OTS were two times as deep as the MFS (CoS/MFS: 2.12 ± 0.2 and OTS/MFS: 2.13 ± 0.3) as in our in-vivo measurements (2.16 and 2.13, respectively). Thus, we were able to identify the MFS in the single histological sections in all (20/20) hemispheres. Fig. 4 (left) shows example histological sections zoomed on the MFS. These data illustrate that the cytoarchitectonic boundary between FG1 and FG2 occurs within the MFS. The reliability of this cortical border between FG1 and FG2 was determined by titrating the number of GLI profiles used in each block used for calculating the Mahalanobis distance function (Materials and methods). These analyses indicate that the positioning of the FG1/FG2 boundary within the MFS was consistent across block sizes (Fig. 4, right). These two slices are indicative of the general trend as the FG1/FG2 boundary occurred within the MFS in 90% (18/20) of hemispheres. To illustrate both the consistency and variability of these cortical borders across subjects, we show coronal histological sections from eight additional hemispheres (Fig. 5). In each case, the boundary between FG1 and FG2 is located in the MFS.

To further examine the link between the MFS morphology and the FG1/FG2 boundary, we generated cortical surface reconstructions for each subject (Fig. 6a). The morphological pattern types of each hemisphere in the post-mortem sample was representative of those documented in our in-vivo sample (Table 1) where Type 1 patterns occurred 60% of the time (12/20) with A patterns about 1.5 times as frequent as B patterns (1.4 for Type 1; 1.67 for Type II). We then projected FG1 and FG2 from the digitized histological sections onto the brain volume and cortical surface to precisely quantify where the microanatomical transition between FG1 and FG2 occurs within the MFS (Fig. 6). This approach yielded three important findings. First, the cytoarchitectonic transition between FG1 and FG2 occurred within the posterior aspect of the MFS irrespective of morphological differences (Fig. 6a). Second, not all of the MFS contains the FG1/FG2 boundary. Indeed, quantifying the percentage of the MFS containing this FG1/FG2 boundary reveals more overlap within the left (60.0 ± 6.5%) than the right (33.4 ± 7.2%) hemisphere (Fig. 6b). Third, though the extent of the MFS containing the FG1/FG2 boundary varies across hemispheres, the cytoarchitectonic transition occurs in a comparable position within its depth across hemispheres, just 3–4 mm from the fundus (left: 3.00 ± 0.42 mm; right: 3.71 ± 0.58 mm; Fig. 6c). Notably, the distance between the entire FG1/FG2 boundary (not just the portion within the MFS as in Fig. 6b) and the MFS in all 20 hemispheres, is on the order of 5 mm (L: 5.75 ± 3.11 mm; R: 5.07 ± 1.07 mm), which is twice as precise as that predicted by Talairach coordinates of the MFS (L: 11.35 ± 1.51 mm; R: 11.65 ± 2.59 mm; $p < 10^{-3}$). Taken together, these analyses reveal that in 90% of hemispheres, nearly half of the FG1/FG2 boundary occurs within the MFS less than 4 mm from the fundus, illustrating a tight correspondence between a microanatomical transition and a macroanatomical landmark within the posterior FG.

Function

The MFS identifies a lateral–medial transition in the eccentricity bias map across age groups

While cytoarchitectonic analyses offer unprecedented precision of micron level measurements elucidating the fine-scale anatomical

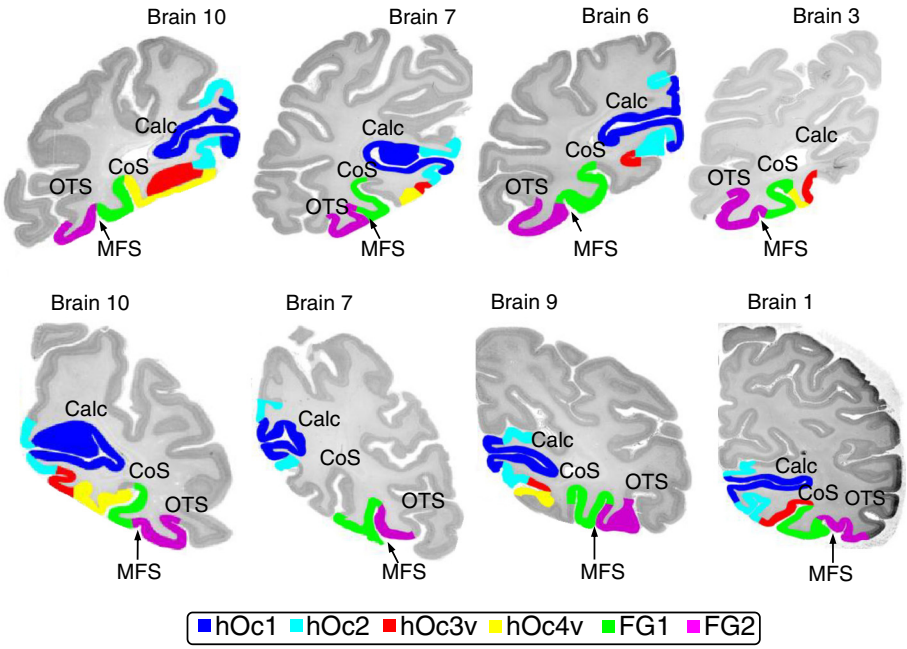

Fig. 5. The MFS identifies the cytoarchitectonic boundary between FG1/FG2. 8 example histological sections from 6 of the 10 brains within which FG1 and FG2 have been defined. Arrows indicate location of the MFS. Legend indicates color code for cytoarchitectonically defined regions hOc1, hOc2, hOc3v, hOc4v, FG1, and FG2. hOc1 and hOc2: from Amunts et al. (2000). hOc3v and hOc4v: from Rottschy et al. (2007). FG1 and FG2: from Caspers et al. (2012). h indicates that the area is defined in the human brain, and Oc indicates that it is in the occipital lobe. Calc: calcarine sulcus; CoS: collateral sulcus; FG: fusiform gyrus; MFS: mid-fusiform sulcus; OTS: occipito-temporal sulcus.

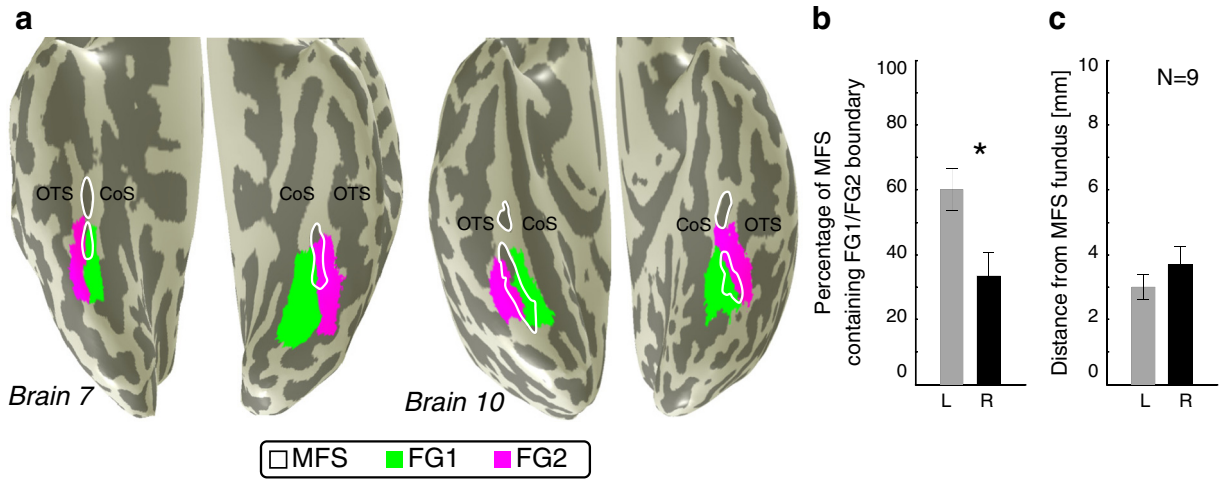

Fig. 6. The boundary between FG1/FG2 occurs within the posterior extent of the MFS less than 4 mm from the fundus. (a) Inflated cortical surfaces from two example postmortem brains showing the entire surface of VTC as well as the FG1 and FG2 cytoarchitectonic regions. White: MFS; green: FG1; magenta: FG2. (b) Percentage of the MFS containing the FG1/FG2 boundary; *Left > right, $p < .01$. (c) Average distance of the FG1/FG2 boundary from the MFS fundus. CoS: collateral sulcus; MFS: mid-fusiform sulcus; OTS: occipito-temporal sulcus.

structure within the shallow MFS, fMRI offers the opportunity to examine the relationship between the MFS and the large-scale functional structure surrounding it. For instance, prior studies show that the MFS separates face-selective regions in lateral VTC from place-selective regions in medial VTC (Nasr et al., 2011; Weiner and Grill-Spector, 2010; Weiner et al., 2010). Given this structural–functional relationship, and the present findings indicating the stability of the MFS across development and its consistent relation to cytoarchitectonic partitions of the FG, we hypothesized that a) the location of the MFS will predict additional functional differentiations between lateral and medial VTC, and b) this relationship will be stable across development.

We tested this hypothesis with eccentricity bias measurements, which show a lateral–medial functional gradient in VTC (Hasson et al., 2002; Levy et al., 2001) and are thought to reflect a general organizing principle of human high-level visual cortex (Malach et al., 2002). Blind to the functional data, we first defined lateral and medial anatomical VTC ROIs guided by the MFS morphology in each subject and hemisphere (Materials and methods). We then used a linear discriminant classifier within and across age groups to determine if the *anatomical* location of VTC functional voxels in one subject's brain could be predicted from learning the structural–functional relationship between anatomy and eccentricity bias in other subjects' brains. Results show that the classifier predicted the anatomical location of voxels significantly above chance in all age groups (all $ts > 45.4$, $ps < 10^{-13}$, Fig. 7b). The percentage voxels classified correctly was 80.2 ± 6.1% (std) in children, 79.5 ± 5.6% in adolescents, and 80.4 ± 5.3% in adults, with no significant differences across age groups (1-way ANOVA, $F(2,35) = .09$, $p = .92$). Intriguingly, anatomical classification across age groups was also significantly above chance (all $ts > 19.84$, $ps < 10^{-10}$) with the average correct classification ranging between 77.3 ± 4.8% and 81.5 ± 5.6% (Fig. 7c). This across age group classification was strikingly similar to within age group classification where a 2-way ANOVA using training age group and testing age group as factors showed no main effect of testing age group ($p = .33$), no main effect of training age group ($p = .18$), and no interaction ($p = .99$). These data reveal a tight structural–functional coupling relative to the MFS across age groups.

To verify the classification results, we projected the eccentricity map of each subject onto their corresponding cortical surface reconstruction. Even though the MFS was not used in the classification analyses, we include the MFS in the visualizations to relate to the distance measurements in Fig. 8, lower right. Consistent with the classification results, there was a clear eccentricity gradient arranged in a reliable manner relative to the MFS. In children, adolescents, and adults, a majority of voxels medial to the MFS showed a clear peripheral bias (cool colors in Fig. 8) and a majority of voxels lateral to the MFS showed a more foveal eccentricity preference (warm colors in Fig. 8). A minority of voxels showed the reverse preference (e.g. voxels with a peripheral bias laterally and a foveal bias medially) in lateral and medial VTC, which

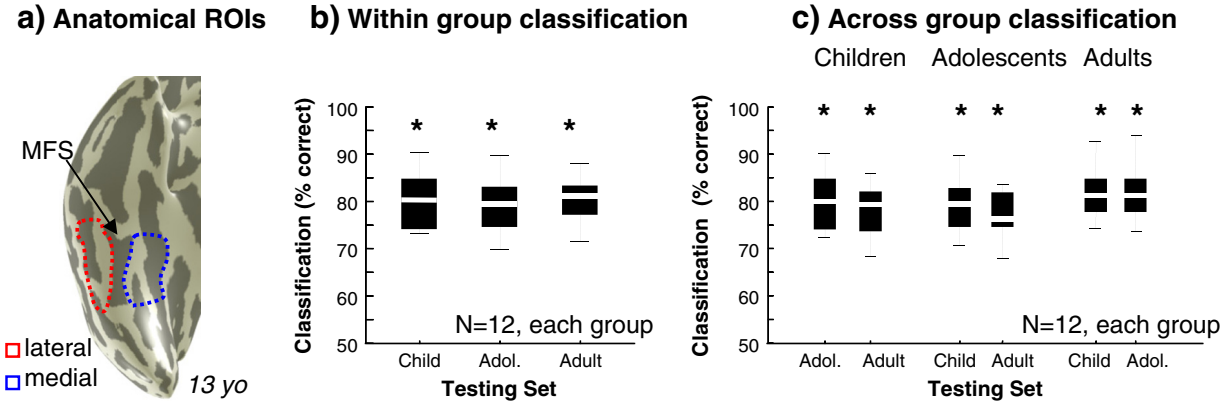

Fig. 7. Classifying structural-functional relationships across age groups. (a) Inflated right hemisphere from an example subject. Blind to functional data, anatomical ROIs were defined lateral and medial to the MFS. (b) Within-group classification performance using a linear discriminant analysis (LDA) with a leave-one-out procedure. Within each age group, classification performance was significantly greater than chance (50%; $p < 10^{-13}$). (c) Across-group classification performance. The LDA was conducted by training on data from one age group and testing with data from each subject in the other age groups. Testing performance was above chance ($p < 10^{-10}$) for all classifications.

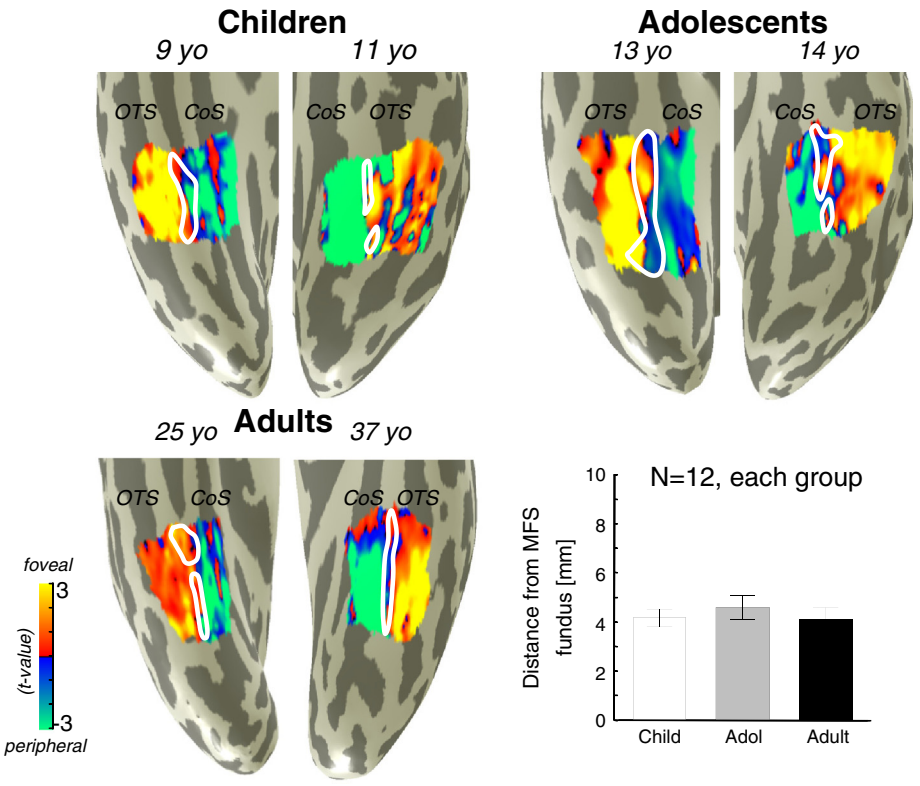

Fig. 8. The MFS identifies a large-scale division in eccentricity bias representations across age groups where the transition from foveal- to peripheral-biased voxels occurs 4 mm from the MFS fundus. Eccentricity bias measurements within the lateral and medial anatomical ROIs were mapped to the cortical surface to visualize the functional distinctions learned by the classifier. As illustrated in example right and left hemispheres from each age group, a majority of voxels lateral to the MFS (white outline) illustrates a foveal bias (warm colors), while a majority of voxels medial to the MFS illustrates a peripheral bias (cool colors). Lower right: Average distance between the MFS fundus and transition of eccentricity bias representation averaged across subjects and hemispheres. CoS: collateral sulcus; MFS: mid-fusiform sulcus; OTS: occipito-temporal sulcus.

explains why the classifier misidentified about 20% of the voxels across age groups (Figs. 7b–c). Intriguingly, the transition of the eccentricity bias map oftentimes occurs within or on the outer lips of the MFS itself (Fig. 8). Measuring the distance between the MFS fundus and the foveal–peripheral transition of the VTC eccentricity bias map (Fig. 8, lower right) reveals that this distance is only 4.1–4.6 mm across age groups (mean and SEM: kids: 4.17 mm ± 0.36 mm; adolescents: 4.58 mm ± 0.51 mm; adults: 4.10 mm ± 0.49 mm), which is comparable to the distance between the MFS fundus and the FG1/FG2 cytoarchitectonic transition. Together, these results indicate a stable structural–functional relationship between the MFS and a large-scale functional map extending from lateral to medial VTC across ages (from 7 to 40, the youngest and oldest subjects in our fMRI study, respectively).

Fine-scale: the anterior tip of the MFS identifies mFus-faces/FFA-2

Can the MFS identify fine-scale functional clusters in addition to transitions in large-scale functional maps?. Prior HR-fMRI studies report two separate face-selective regions along the length of the MFS where one overlaps anterior portions of the MFS extending into the lateral FG (mFus-faces/FFA-2) and another overlaps the posterior portion of the MFS and lateral FG extending into the OTS (pFus-faces/FFA-1) adjacent to a body part-selective region (OTS-limbs/FBA: Weiner and Grill-Spector, 2010, 2011, 2012, 2013; Weiner et al., 2010; Figs. 9–10). However, the exact correspondence of mFus-faces/FFA-2 and pFus-faces/FFA-1 with respect to the morphological features of the MFS (Figs. 1–2) has not been quantified. We examined two possible outcomes. One possibility is that there is a direct relationship between the morphological features of the MFS and the location of face-selective regions, suggesting that their location will be determined by the anterior and posterior ends of the MFS, respectively. Alternatively, given the greater variability in the posterior than anterior aspect of the MFS (see Results—Morphology), there may be a stronger coupling between the anterior tip of the MFS and mFus-faces/FFA-2 than between the posterior tip and pFus-faces/FFA-1.

In order to quantify the structural–functional coupling between the MFS and face-selective regions, we positioned 1 cm disks at the anterolateral and posterolateral limits of the MFS in each hemisphere and determined the amount of overlap between these disks and face-selective ROIs (Fig. 9; Materials and methods). Our measurements reveal that the strongest functional–structural coupling occurs between the anterolateral tip of the right MFS and right mFus-faces/FFA-2 (Fig. 9). Strikingly, 83 ± 7% of the right mFus-faces/FFA-2 is located within a 1 cm anatomical disk located on the anterior tip of the MFS (left: 66 ± 7%; significantly less than right $t(13) = 2.4$, $p < .03$). Notably, and in support of the second hypothesis, the coupling between the anterolateral tip of the MFS and mFus-faces/FFA-2 is significantly stronger than the coupling between the posterolateral tip of the MFS and pFus-faces/FFA-1 which is about 50% (left: 50 ± 9%; right: 48 ± 9%; two-way repeated measures ANOVA with factors region and hemisphere revealing a significant main effect of region $F(1,13) = 10.74$, $p < .006$). Critically, identifying the functional–structural coupling between face-selective regions and the MFS is more than twice as effective compared to the coupling of face-selective regions with Talairach coordinates. That is, repeating the same analysis with 1 cm disk ROIs placed on the published Talairach coordinates of FFA-1 and FFA-2 (Pinsk et al., 2009) produces an average coupling of only 18 ± 4% with each functional ROI (dashed lines in Fig. 9). Thus, MFS-functional coupling is significantly better than Talairach-functional coupling (two-way repeated measures ANOVA using as factors ROI type (anatomical vs. Talairach) and hemisphere, showing a significant main effect of ROI type: $F(1,13) = 31.04$,

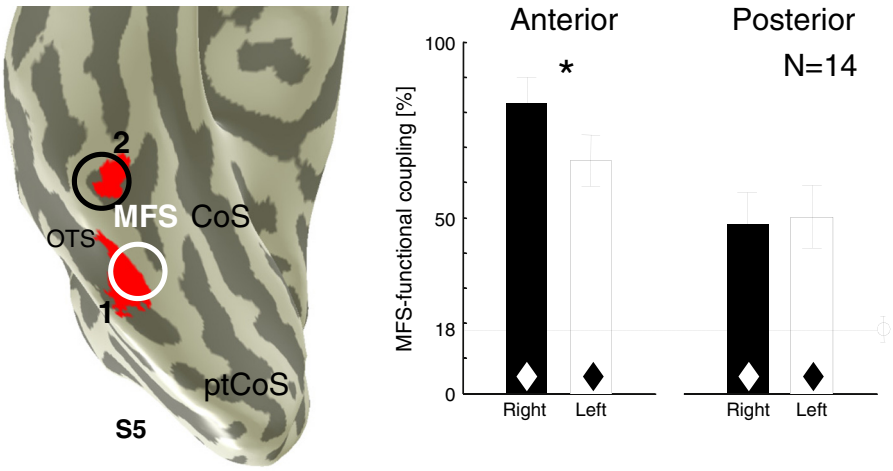

Fig. 9. Structural-functional coupling is highest in the anterior tip of the MFS. Left: Inflated right cortical surface from one example subject. Red illustrates face-selective voxels corresponding to mFus-faces/FFA-2 (2) and pFus-faces/FFA-1 (1). Disks illustrate positioning of anatomical ROIs. Each disk was 1 cm in diameter and positioned at the anterolateral (black) or posterolateral (white) tip of the MFS extending to the lateral FG. Right: Bars: Proportion of face-selective voxels that are contained within the anatomical disk ROIs described in image at left. Dashed line: Proportion of face-selective voxels that are contained within Talairach-defined disks centered on the coordinates of FFA-1 and FFA-2 from Pinsk et al. (2009). *Right > left, $p < .03$. ♦ MFS-functional coupling > Talairach-functional coupling, $p < .02$. CoS: collateral sulcus; MFS: mid–fusiform sulcus; OTS: occipito-temporal sulcus; ptCoS: posterior transverse collateral sulcus.

$p < .0001$). Together, these results reveal that irrespective of MFS type or length, the MFS is a stable identifier for mFus-faces/FFA-2, less so for pFus-faces/FFA-1, and both significantly better than Talairach coordinates.

To link these measurements to MFS morphology and the location of these regions relative to other macroanatomical landmarks such as OTS, CoS, and ptCoS, we illustrate four example hemispheres with various MFS morphological patterns (Fig. 10; IOG-faces/OFA and OTS-limbs/FBA are also included to anchor the reader). Despite differences in morphological patterns, the anterior tip of the MFS (white in Fig. 10) is coupled with mFus-faces/FFA-2. In the case of pFus-faces/FFA-1, the relation is less salient. In some brains the posterior tip of the MFS aligns with pFus-faces/FFA-1 (Subjects 1 and 3). However, in brains with a short MFS, the posterior tip of the MFS does not align with pFus-faces/FFA-1 (Subject 2). These data indicate that the anterior extent of the MFS is a stable macroanatomical landmark predicting the location of mFus-faces/FFA-2 independent of MFS morphology.

Discussion

The present findings provide empirical evidence demonstrating that the mid-fusiform sulcus (MFS) is a key macroanatomical landmark identifying both cytoarchitectonic and functional divisions of human ventral temporal cortex (VTC). Macroanatomically, the MFS is a shallow sulcus dividing the fusiform gyrus (FG) longitudinally and appears as one of four morphological patterns irrespective of age, gender, or hemisphere (Figs. 1–3). Identifying the MFS in histological sections illustrates that the boundary between two cytoarchitectonic regions, FG1 and FG2, occurs within the sulcal bed of the posterior MFS (Figs. 4–6). Additionally, the MFS shows tight structural–functional coupling at both large and fine spatial scales. At a large-scale, the MFS is a landmark identifying a lateral–medial functional transition in the eccentricity bias map in children, adolescents, and adults (Figs. 7–8). At a fine-scale, the MFS identifies an anterior–posterior anatomical differentiation of two fusiform face-selective regions where the anterior tip of the MFS most

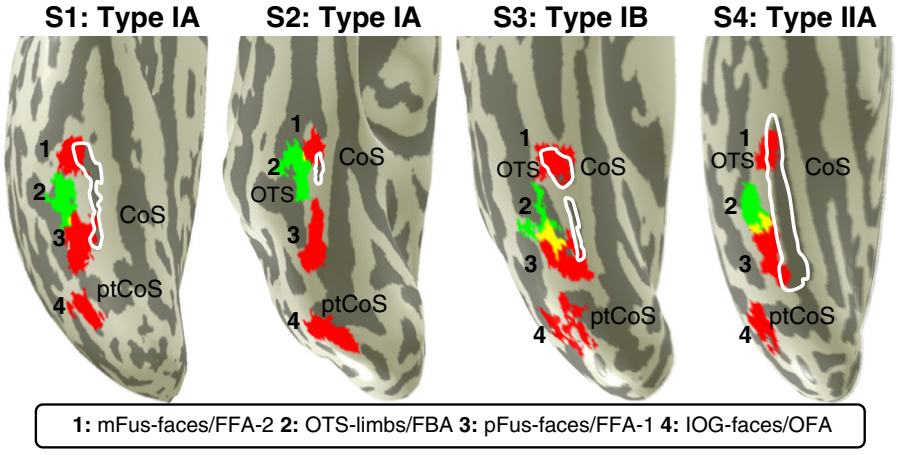

Fig. 10. The MFS identifies a fine-scale division of face-selective regions irrespective of morphology. Face- (red) and limb-selective (green) parameter maps, as well as their overlap (yellow), as measured with high-resolution fMRI on four example right hemispheres with three different MFS morphological patterns. Irrespective of type or length in a given hemisphere, the MFS separates mFus-faces/FFA-2 from pFus-faces/FFA-1 along the length of the FG, where the anterior portion of the MFS tightly couples with mFus-faces/FFA-2 across subjects. CoS: collateral sulcus; OTS: occipito-temporal sulcus; ptCoS: posterior transverse collateral sulcus; MFS outlined in white. Red: faces > nonfaces, $t > 3$; green: limbs > nonlimbs, $t > 3$; yellow: overlap.

tightly couples with mFus-faces/FFA-2 (Figs. 9–10). In the sections below, we discuss how the correspondence of a macroanatomical landmark with both cytoarchitectonic and functional parcellations may develop in high-level sensory cortex and the implications of this correspondence for future research.

Stable morphological features of the MFS across children, adolescents, and adults

In the original observation of the MFS in modern writing, Puce et al. (1996) reported, "The fusiform gyrus often is divided by a longitudinal sulcus that can be confused with the collateral sulcus in isolated coronal slices" (p. 5207). Seventeen years later, our findings clarify the morphology of the MFS, identifying its shallowness as its hallmark morphological feature which discriminates it from the surrounding OTS and CoS. The difference in depth among these three sulci generates a distinctive "ω" pattern on coronal slices, which is identifiable from age 7 to 85 (the youngest and oldest subjects of our four studies, respectively). The stability of the MFS morphology across development makes it a particularly useful landmark to incorporate into studies examining the functional properties of the FG across age groups and populations (Cantlon et al., 2011; Golarai et al., 2006, 2007, 2010a, 2010b; Grill-Spector et al., 2008; Peelen et al., 2009; Scherf et al., 2007), as well as histological studies across typical (Caspers et al., 2012) and atypical (Courchesne et al., 2005; van Kooten et al., 2008) populations. It would be particularly interesting to investigate if the MFS is present in newborns and if the structural–functional coupling we report here is already evident at birth. Importantly, identifying the MFS may (1) increase the precision of anatomical registration across subjects by increasing the inter-rater reliability of manual identification of sulci, which is lowest in VTC (Sowell et al., 2002), (2) improve the alignment among brains in atlasing projects using large cohorts of subjects (Van Essen et al., 2012a, 2012b), and (3) aid investigations of functional–structural correspondences using cortex based alignment methods (CBA; Frost and Goebel, 2012, 2013). While present studies applying CBA report substantial variability in the cortical positioning of functional regions along the length of the lateral FG (Frost and Goebel, 2012, 2013), inclusion of the MFS in future CBA techniques may substantially reduce this variability.

The MFS is a landmark identifying cytoarchitectonic and functional divisions of VTC

Understanding the morphology of the MFS allowed us to link cortical folding patterns to both cytoarchitectonic and functional divisions of the FG. Interestingly, both the cytoarchitectonic division between FG1 and FG2 and the functional division among peripheral and foveal representations occur along a medial–lateral axis relative to the MFS. That is, FG1 and peripherally–biased voxels are located within the medial aspect of the MFS extending into the medial FG and CoS, whereas FG2 and foveally–biased voxels are located within the lateral aspect of the MFS extending into the lateral FG and OTS. Given that cytoarchitectonic (FG1/FG2) and functional representations (peripheral-bias/foveal-bias) occupy the same macroanatomical expanse on either side of the MFS, and both within comparable distances from the MFS fundus on the order of 4 mm within the MFS itself, our results suggest that differential neural hardware may implement differential computations on medial and lateral aspects of VTC. Our findings also raise new questions regarding the relationship between the underlying neural architecture with the functional properties of these regions. For instance: *Is the peripheral bias in medial VTC an outcome of the defining features of FG1, such as its columnar organization? How is the foveal bias in lateral VTC associated with the defining features of FG2, such as its lack of a columnar organization and increased neuronal density compared to FG1?*

From structure to function: implications for cytoarchitectonic–functional coupling in VTC

Linking between cytoarchitectonic and functional divisions of VTC through their correspondence to the MFS is not limited to foveal and peripheral biases, but may extend to other large-scale maps and fine-scale clusters identified in VTC. For instance, recent fMRI studies in adults show that face- and place-selective regions are also reliably separated by the MFS (Nasr et al., 2011; Weiner and Grill-Spector, 2010; Weiner et al., 2010) indicating the generality of the MFS as a functional landmark in VTC. In addition to eccentricity bias and category selectivity, lateral–medial functional gradients have also been found for animacy (Connolly et al., 2012; Kriegeskorte et al., 2008; Mahon et al., 2009; Martin, 2007), real-world object size (Konkle and Oliva, 2012), semantics (Huth et al., 2012), and retinotopy (Arcaro et al., 2009; Brewer et al., 2005; Kolster et al., 2010). Since the boundary of FG1 and FG2 occurs within the MFS, we predict that a functional component of each of these maps will align with respect to the MFS, which can be directly tested in future studies.

While our data suggest differential neural architectures on separate sides of the MFS, we caution that the correspondence between cytoarchitectonic and functional divisions are likely not one-to-one. First, while all of the maps mentioned above display a similar lateral–medial gradient, these maps are not identical in their spatial organization across the cortical sheet. For example, though the cortical representations differentiating faces from scenes and foveal from peripheral biases both illustrate a lateral–medial gradient, respectively, they do not overlap entirely (Hasson et al., 2002; Levy et al., 2001, 2004; Malach et al., 2002). Second, within these large-scale maps, the MFS-functional coupling may be different for fine-scale clusters. In the present study, we illustrated this with face-selective regions where there is a tighter correspondence between the MFS and mFus-faces/FFA-2 than for pFus-faces/FFA-1 (Fig. 9). However, there are additional fine-scale clusters in both lateral VTC (e.g. for limbs, words, and objects: Grill-Spector, 2003; Peelen and Downing, 2007; Weiner and Grill-Spector, 2013; Yeatman et al., 2012) and medial VTC (e.g. several retinotopic maps: Arcaro et al., 2009; Brewer et al., 2005), making it highly probable that FG1 and FG2 each contain several fine-scale functional regions. Future research will determine how these many large-scale maps and fine-scale clusters tile cytoarchitectonic regions, as well as directly relate their overlapping and non-overlapping portions to the specific neural hardware of FG1 or FG2. Recent methodological advancements in non-invasive quantitative measurements of cortical anatomy, such as myeloarchitecture (Dick et al., 2012; Glasser and Van Essen, 2011; Mezer et al., in press; Sereno et al., 2013), and subvoxel fMRI acquisitions (Zimmermann et al., 2011), might make this possible and may allow researchers to directly relate microarchitectural and functional boundaries within the same subjects.

What mechanisms may generate the cortical folding of the MFS and its correspondence with cytoarchitechtonic and functional parcellations of VTC?

Several hypotheses (Zilles et al., 2013) have been proposed to explain the formation of cortical folding, including cell migration (Rakic, 1995, 2009), inhomogeneous cell growth across cortical layers (Richman et al., 1975), and tension generated by axonal connectivity in white matter (Van Essen, 1997). Interestingly, the tension-based hypothesis (Van Essen, 1997) suggests that strongly connected regions will be located on different sides of a gyrus and that sulci may form from region-specific tensions pulling in opposite directions. Since both cytoarchitectonic regions FG1 and FG2 (as well as peripherally- and foveally-biased representations as measured in the present study) wrap around separate gyral components flanking the MFS, the tension-based hypothesis predicts higher connectivity within than between FG1 and FG2, which in turn generates a pull forming the MFS. Likewise, the

model predicts higher connectivity within peripherally-biased representations medial to the MFS than between foveally- and peripherally-biased representations on different sides of the MFS. According to this scenario, the cortical folding of the MFS is a consequence of an interplay among cytoarchitectonic, connectivity, and functional demands. As the aforementioned theories of cortical folding (Rakic, 1995, 2009; Richman et al., 1975; Van Essen, 1997) are not mutually exclusive (Zilles et al., 2013), future work is needed to shed light on how combinations of these proposed mechanisms may explain differing relationships of macroanatomical landmarks with cytoarchitectonic and functional parcellations throughout the cerebral cortex.

Summary

In conclusion, the present study implemented a novel multimodal approach, combining measurements across macroanatomics, cytoarchitectonics, as well as both standard and high-resolution fMRI for the first time in human VTC. This unique method revealed that the mid-fusiform sulcus (MFS) is a macroanatomical landmark in human VTC identifying 1) a cytoarchitectonic lateral–medial division between areas FG1 and FG2, 2) a functional lateral–medial transition in a large-scale eccentricity bias map across age groups, and 3) an anterior–posterior discrimination of mFus-faces/FFA-2 from pFus-faces/FFA-1. We hypothesize that the lateral–medial cytoarchitectonic transition within the MFS provides a mechanistic explanation for the pervasive lateral–medial functional divisions of VTC more generally. Future studies will determine if other sensory and non-sensory cortical regions also exhibit a similar relationship among macroanatomical, cytoarchitectonical, and functional organization, or if this correspondence is specific to human ventral temporal cortex.

Acknowledgments

This research was funded by NSF BCS0920865, NIH 1 RO1 EY 02231801A1, the Initiative and Networking Fund of the Helmholtz Association within the Helmholtz Alliance on Systems Biology (Human Brain Model), and the DFG (IRTG 1328). We thank Alina Liberman, Yotam de la Zerda, and David Loftus for help with manually segmenting anatomical brain volumes, as well as Kendrick Kay for advice on fMRI analyses.

Conflicts of interest

None.

References

Aguirre, G.K., Zarahn, E., D'Esposito, M., 1998. An area within human ventral cortex sensitive to "building" stimuli: evidence and implications. Neuron 21, 373–383.
Allison, T., Puce, A., Spencer, D.D., McCarthy, G., 1999. Electrophysiological studies of human face perception. I: Potentials generated in occipitotemporal cortex by face and non-face stimuli. Cereb. Cortex 9, 415–430.
Amedi, A., Jacobson, G., Hendler, T., Malach, R., Zohary, E., 2002. Convergence of visual and tactile shape processing in the human lateral occipital complex. Cereb. Cortex 12, 1202–1212.
Amunts, K., Zilles, K., 2001. Advances in cytoarchitectonic mapping of the human cerebral cortex. Neuroimaging Clin. N. Am. 11, 151–169 (vii).
Amunts, K., Schleicher, A., Burgel, U., Mohlberg, H., Uylings, H.B., Zilles, K., 1999. Broca's region revisited: cytoarchitecture and intersubject variability. J. Comp. Neurol. 412, 319–341.
Amunts, K., Malikovic, A., Mohlberg, H., Schormann, T., Zilles, K., 2000. Brodmann's areas 17 and 18 brought into stereotaxic space—where and how variable? NeuroImage 11, 66–84.
Amunts, K., Weiss, P.H., Mohlberg, H., Pieperhoff, P., Eickhoff, S., Gurd, J.M., Marshall, J.C., Shah, N.J., Fink, G.R., Zilles, K., 2004. Analysis of neural mechanisms underlying verbal fluency in cytoarchitectonically defined stereotaxic space—the roles of Brodmann areas 44 and 45. NeuroImage 22, 42–56.
Amunts, K., Kedo, O., Kindler, M., Pieperhoff, P., Mohlberg, H., Shah, N.J., Habel, U., Schneider, F., Zilles, K., 2005. Cytoarchitectonic mapping of the human amygdala, hippocampal region and entorhinal cortex: intersubject variability and probability maps. Anat. Embryol. (Berl) 210, 343–352.
Arcaro, M.J., McMains, S.A., Singer, B.D., Kastner, S., 2009. Retinotopic organization of human ventral visual cortex. J. Neurosci. 29, 10638–10652.
Brewer, A.A., Liu, J., Wade, A.R., Wandell, B.A., 2005. Visual field maps and stimulus selectivity in human ventral occipital cortex. Nat. Neurosci. 8, 1102–1109.
Brodmann, K., 1909. Vergleichende Lokalisationslehre der Grosshirnrinde in ihren Prinzipien dargestellt auf Grund des Zellenbaues. Johann Ambrosius Barth Verlag, Leipzig, Germany.
Cantlon, J.F., Pinel, P., Dehaene, S., Pelphrey, K.A., 2011. Cortical representations of symbols, objects, and faces are pruned back during early childhood. Cereb. Cortex 21, 191–199.
Caspers, J., Zilles, K., Eickhoff, S.B., Schleicher, A., Mohlberg, H., Amunts, K., 2012. Cytoarchitectonical analysis and probabilistic mapping of two extrastriate areas of the human posterior fusiform gyrus. Brain Struct. Funct. 218 (2), 511–526.
Connolly, A.C., Guntupalli, J.S., Gors, J., Hanke, M., Halchenko, Y.O., Wu, Y.C., Abdi, H., Haxby, J.V., 2012. The representation of biological classes in the human brain. J. Neurosci. 32, 2608–2618.
Courchesne, E., Redcay, E., Morgan, J.T., Kennedy, D.P., 2005. Autism at the beginning: microstructural and growth abnormalities underlying the cognitive and behavioral phenotype of autism. Dev. Psychopathol. 17, 577–597.
Davidenko, N., Remus, D.A., Grill-Spector, K., 2012. Face-likeness and image variability drive responses in human face-selective ventral regions. Hum. Brain Mapp. 33, 2334–2349.
Dick, F., Tierney, A.T., Lutti, A., Josephs, O., Sereno, M.I., Weiskopf, N., 2012. In vivo functional and myeloarchitectonic mapping of human primary auditory areas. J. Neurosci. 32, 16095–16105.
Duvernoy, H., 1999. The Human Brain: Surface, Blood Supply, and Three-Dimensional Sectional Anatomy. Springer, Vienna.
Epstein, R., Kanwisher, N., 1998. A cortical representation of the local visual environment. Nature 392, 598–601.
Evans, A.C., Marrett, S., Neelin, P., Collins, L., Worsley, K., Dai, W., Milot, S., Meyer, E., Bub, D., 1992. Anatomical mapping of functional activation in stereotactic coordinate space. NeuroImage 1, 43–53.
Frost, M.A., Goebel, R., 2012. Measuring structural–functional correspondence: spatial variability of specialised brain regions after macro-anatomical alignment. NeuroImage 59, 1369–1381.
Frost, M.A., Goebel, R., 2013. Functionally informed cortex based alignment: an integrated approach for whole-cortex macro-anatomical and ROI-based functional alignment. NeuroImage.
Glasser, M.F., Van Essen, D.C., 2011. Mapping human cortical areas in vivo based on myelin content as revealed by T1- and T2-weighted MRI. J. Neurosci. 31, 11597–11616.
Glover, G.H., 1999. Simple analytic spiral K-space algorithm. Magn. Reson. Med. 42, 412–415.
Golarai, G., Grill-Spector, K., Reiss, A.L., 2006. Autism and the development of face processing. Clin. Neurosci. Res. 6, 145–160.
Golarai, G., Ghahremani, D.G., Whitfield-Gabrieli, S., Reiss, A., Eberhardt, J.L., Gabrieli, J.D., Grill-Spector, K., 2007. Differential development of high-level visual cortex correlates with category-specific recognition memory. Nat. Neurosci. 10, 512–522.
Golarai, G., Liberman, A., Yoon, J.M., Grill-Spector, K., 2010a. Differential development of the ventral visual cortex extends through adolescence. Front. Hum. Neurosci. 3, 80.
Golarai, G., Hong, S., Haas, B.W., Galaburda, A.M., Mills, D.L., Bellugi, U., Grill-Spector, K., Reiss, A.L., 2010b. The fusiform face area is enlarged in Williams syndrome. J. Neurosci. 30, 6700–6712.
Grill-Spector, K., 2003. The neural basis of object perception. Curr. Opin. Neurobiol. 13, 159–166.
Grill-Spector, K., Golarai, G., Gabrieli, J., 2008. Developmental neuroimaging of the human ventral visual cortex. Trends Cogn. Sci. 12, 152–162.
Hasson, U., Levy, I., Behrmann, M., Hendler, T., Malach, R., 2002. Eccentricity bias as an organizing principle for human high-order object areas. Neuron 34, 479–490.
Haxby, J.V., Hoffman, E.A., Gobbini, M.I., 2000. The distributed human neural system for face perception. Trends Cogn. Sci. 4, 223–233.
Henson, R., Shallice, T., Dolan, R., 2000. Neuroimaging evidence for dissociable forms of repetition priming. Science 287, 1269–1272.
Huntgeburth, S.C., Petrides, M., 2012. Morphological patterns of the collateral sulcus in the human brain. Eur. J. Neurosci. 35, 1295–1311.
Huth, A.G., Nishimoto, S., Vu, A.T., Gallant, J.L., 2012. A continuous semantic space describes the representation of thousands of object and action categories across the human brain. Neuron 76, 1210–1224.
James, T.W., Humphrey, G.K., Gati, J.S., Servos, P., Menon, R.S., Goodale, M.A., 2002. Haptic study of three-dimensional objects activates extrastriate visual areas. Neuropsychologia 40, 1706–1714.
Kanwisher, N., McDermott, J., Chun, M.M., 1997. The fusiform face area: a module in human extrastriate cortex specialized for face perception. J. Neurosci. 17 (11), 4302-4011.
Kitada, R., Johnsrude, I.S., Kochiyama, T., Lederman, S.J., 2009. Functional specialization and convergence in the occipito-temporal cortex supporting haptic and visual identification of human faces and body parts: an fMRI study. J. Cogn. Neurosci. 21, 2027–2045.
Kolster, H., Peeters, R., Orban, G.A., 2010. The retinotopic organization of the human middle temporal area MT/V5 and its cortical neighbors. J. Neurosci. 30, 9801–9820.
Konkle, T., Oliva, A., 2012. A real-world size organization of object responses in occipitotemporal cortex. Neuron 74, 1114–1124.
Kriegeskorte, N., Mur, M., Ruff, D.A., Kiani, R., Bodurka, J., Esteky, H., Tanaka, K., Bandettini, P.A., 2008. Matching categorical object representations in inferior temporal cortex of man and monkey. Neuron 60, 1126–1141.
Levy, I., Hasson, U., Avidan, G., Hendler, T., Malach, R., 2001. Center–periphery organization of human object areas. Nat. Neurosci. 4, 533–539.
Levy, I., Hasson, U., Harel, M., Malach, R., 2004. Functional analysis of the periphery effect in human building related areas. Hum. Brain Mapp. 22 (1), 15–26.

Mahon, B.Z., Caramazza, A., 2009. Concepts and categories: a cognitive neuropsychological perspective. Annu. Rev. Psychol. 60, 27–51.
Mahon, B.Z., Anzellotti, S., Schwarzbach, J., Zampini, M., Caramazza, A., 2009. Category-specific organization in the human brain does not require visual experience. Neuron 63, 397–405.
Malach, R., Levy, I., Hasson, U., 2002. The topography of high-order human object areas. Trends Cogn. Sci. 6, 176–184.
Martin, A., 2007. The representation of object concepts in the brain. Annu. Rev. Psychol. 58, 25–45.
Merker, B., 1983. Silver staining of cell bodies by means of physical development. J. Neurosci. Methods 9, 235–241.
Mezer, A., Yeatman, J.D., Wandell, B.A., 2013. Quantifying the local tissue volume and composition in individual brains with MRI. Nat. Med. (in press).
Nasr, S., Liu, N., Devaney, K.J., Yue, X., Rajimehr, R., Ungerleider, L.G., Tootell, R.B., 2011. Scene-selective cortical regions in human and nonhuman primates. J. Neurosci. 31, 13771–13785.
Nestares, O., Heeger, D.J., 2000. Robust multiresolution alignment of MRI brain volumes. Magn. Reson. Med. 43, 705–715.
Nobre, A.C., Allison, T., McCarthy, G., 1998. Modulation of human extrastriate visual processing by selective attention to colours and words. Brain 121 (Pt 7), 1357–1368.
Ono, M., Kubik, S., Abernathey, C., 1990. Atlas of the Cerebral Sulci. Thieme, Stuttgart.
Op de Beeck, H.P., Haushofer, J., Kanwisher, N.G., 2008. Interpreting fMRI data: maps, modules and dimensions. Nat. Rev. Neurosci. 9, 123–135.
Parvizi, J., Jacques, C., Foster, B.L., Withoft, N., Rangarajan, V., Weiner, K.S., Grill-Spector, K., 2012. Electrical stimulation of human fusiform face-selective regions distorts face perception. J. Neurosci. 32, 14915–14920.
Peelen, M.V., Downing, P.E., 2007. The neural basis of visual body perception. Nat. Rev. Neurosci. 8, 636–648.
Peelen, M.V., Glaser, B., Vuilleumier, P., Eliez, S., 2009. Differential development of selectivity for faces and bodies in the fusiform gyrus. Dev. Sci. 12, F16–F25.
Pinsk, M.A., Arcaro, M., Weiner, K.S., Kalkus, J.F., Inati, S.J., Gross, C.G., Kastner, S., 2009. Neural representations of faces and body parts in macaque and human cortex: a comparative FMRI study. J. Neurophysiol. 101, 2581–2600.
Puce, A., Allison, T., Asgari, M., Gore, J.C., McCarthy, G., 1996. Differential sensitivity of human visual cortex to faces, letterstrings, and textures: a functional magnetic resonance imaging study. J. Neurosci. 16, 5205–5215.
Rakic, P., 1995. A small step for the cell, a giant leap for mankind: a hypothesis of neocortical expansion during evolution. Trends Neurosci. 18, 383–388.
Rakic, P., 2009. Evolution of the neocortex: a perspective from developmental biology. Nat. Rev. Neurosci. 10, 724–735.
Richman, D.P., Stewart, R.M., Hutchinson, J.W., Caviness, V.S., 1975. Mechanical model of brain convolutional development. Science 189, 18–21.
Rottschy, C., Eickhoff, S.B., Schleicher, A., Mohlberg, H., Kujovic, M., Zilles, K., Amunts, K., 2007. Ventral visual cortex in humans: cytoarchitectonic mapping of two extrastriate areas. Hum. Brain Mapp. 28, 1045–1059.
Scherf, K.S., Behrmann, M., Humphreys, K., Luna, B., 2007. Visual category-selectivity for faces, places and objects emerges along different developmental trajectories. Dev. Sci. 10, F15–F30.
Schleicher, A., Amunts, K., Geyer, S., Morosan, P., Zilles, K., 1999. Observer-independent method for microstructural parcellation of cerebral cortex: a quantitative approach to cytoarchitectonics. NeuroImage 9, 165–177.
Schleicher, A., Palomero-Gallagher, N., Morosan, P., Eickhoff, S.B., Kowalski, T., de Vos, K., Amunts, K., Zilles, K., 2005. Quantitative architectural analysis: a new approach to cortical mapping. Anat. Embryol. (Berl) 210, 373–386.
Schultz, R.T., Grelotti, D.J., Klin, A., Kleinman, J., Van der Gaag, C., Marois, R., Skudlarski, P., 2003. The role of the fusiform face area in social cognition: implications for the pathobiology of autism. Philos. Trans. R. Soc. Lond. B Biol. Sci. 358, 415–427.
Sereno, M.I., Lutti, A., Weiskopf, N., Dick, F., 2013. Mapping the human cortical surface by combining quantitative T1 with retinotopy. Cereb. Cortex 23 (9), 2261–2268.
Sowell, E.R., Thompson, P.M., Rex, D., Kornsand, D., Tessner, K.D., Jernigan, T.L., Toga, A.W., 2002. Mapping sulcal pattern asymmetry and local cortical surface gray matter distribution in vivo: maturation in perisylvian cortices. Cereb. Cortex 12, 17–26.
Talairach, J., Tournoux, P., 1988. Co-planar stereotaxic atlas of the human brain: 3-dimensional proportional system—an approach to cerebral imaging. Thieme, New York.
Tarr, M.J., Gauthier, I., 2000. FFA: a flexible fusiform area for subordinate-level visual processing automatized by expertise. Nat. Neurosci. 3, 764–769.
Van Essen, D.C., 1997. A tension-based theory of morphogenesis and compact wiring in the central nervous system. Nature 385, 313–318.
Van Essen, D.C., Glasser, M.F., Dierker, D.L., Harwell, J., Coalson, T., 2012a. Parcellations and hemispheric asymmetries of human cerebral cortex analyzed on surface-based atlases. Cereb. Cortex 22, 2241–2262.
Van Essen, D.C., Ugurbil, K., Auerbach, E., Barch, D., Behrens, T.E., Bucholz, R., Chang, A., Chen, L., Corbetta, M., Curtiss, S.W., Della Penna, S., Feinberg, D., Glasser, M.F., Harel, N., Heath, A.C., Larson-Prior, L., Marcus, D., Michalareas, G., Moeller, S., Oostenveld, R., Petersen, S.E., Prior, F., Schlaggar, B.L., Smith, S.M., Snyder, A.Z., Xu, J., Yacoub, E., 2012b. The Human Connectome Project: a data acquisition perspective. NeuroImage 62, 2222–2231.
van Kooten, I.A., Palmen, S.J., von Cappeln, P., Steinbusch, H.W., Korr, H., Heinsen, H., Hof, P.R., van Engeland, H., Schmitz, C., 2008. Neurons in the fusiform gyrus are fewer and smaller in autism. Brain 131, 987–999.
Wagner, A.D., Koutstaal, W., Schacter, D.L., 1999. When encoding yields remembering: insights from event-related neuroimaging. Philos. Trans. R. Soc. Lond. B Biol. Sci. 354, 1307–1324.
Wandell, B.A., Chial, S., Backus, B.T., 2000. Visualization and measurement of the cortical surface. J. Cogn. Neurosci. 12, 739–752.
Weiner, K.S., Grill-Spector, K., 2010. Sparsely-distributed organization of face and limb activations in human ventral temporal cortex. NeuroImage 52, 1559–1573.
Weiner, K.S., Grill-Spector, K., 2011. Not one extrastriate body area: using anatomical landmarks, hMT+, and visual field maps to parcellate limb-selective activations in human lateral occipitotemporal cortex. NeuroImage 56, 2183–2199.
Weiner, K.S., Grill-Spector, K., 2012. The improbable simplicity of the fusiform face area. Trends Cogn. Sci. 16, 251–254.
Weiner, K.S., Grill-Spector, K., 2013. Neural representations of faces and limbs neighbor in human high-level visual cortex: evidence for a new organization principle. Psychol. Res. 77, 74–97.
Weiner, K.S., Sayres, R., Vinberg, J., Grill-Spector, K., 2010. fMRI-adaptation and category selectivity in human ventral temporal cortex: regional differences across time scales. J. Neurophysiol. 103, 3349–3365.
Yeatman, J.D., Rauschecker, A.M., Wandell, B.A., 2012. Anatomy of the visual word form area: adjacent cortical circuits and long-range white matter connections. Brain Lang. 125 (2), 146–155.
Zilles, K., Schleicher, A., Palomero-Gallagher, N., Amunts, K., 2002. Quantitative analysis of cyto- and receptor architecture of the human brain. In: Toga, A.W., Mazziotta, J.C. (Eds.), Brain Mapping: The Methods. Academic Press, San Diego, pp. 573–602.
Zilles, K., Palomero-Gallagher, N., Amunts, K., 2013. Development of cortical folding during evolution and ontogeny. Trends Neurosci. 36, 275–284.
Zimmermann, J., Goebel, R., De Martino, F., van de Moortele, P.F., Feinberg, D., Adriany, G., Chaimow, D., Shmuel, A., Ugurbil, K., Yacoub, E., 2011. Mapping the organization of axis of motion selective features in human area MT using high-field fMRI. PLoS One 6, e28716.